Plasmonic absorption enhancement in organic solar cells with thin active layers

Honghui Shen,[a)] Peter Bienstman, and Bjorn Maes

Department of Information Technology (INTEC), Photonics Research Group, Ghent University-IMEC, St-Pietersnieuwstraat 41, 9000 Ghent, Belgium

The influence of silver nanoparticles on light absorption in organic solar cells based on poly(3-exylthiophene):(6,6)-phenyl-C61-butyric-acid-methyl ester is studied by means of finite element method simulations. The metallic nanoparticles are embedded directly inside the active layer. We investigate the enhancement mechanism and the influence of factors such as the spacing between neighboring nanoparticles, the particle diameter, and the coating thickness. The plasmonic resonance of the particles has a wideband influence on the absorption, and we observe a rich interaction between plasmonic enhancement and the absorption characteristics of the active layer material. An enhancement with a factor of around 1.56 is observed for nanoparticles with a diameter of 24 nm and a spacing of 40 nm, bringing the structure to the absorption level of much thicker active layers without nanoparticles. In addition, a significant effect of the particle coating thickness is observed. © *2009 American Institute of Physics.* [doi:10.1063/1.3243163]

I. INTRODUCTION

Organic solar cells (OSCs) are of great current interest as they have a strong potential to reduce the cost of photovoltaics.[1] However, OSCs still have low efficiency, up to 5%–6%,[2,3] due to the short exciton diffusion length. This efficiency is much smaller than commercial silicon-based solar cells. The short exciton diffusion length in OSCs limits the thickness of the active layer. The advanced bulk heterojunction (BHJ) concept was introduced to solve the diffusion length problem and to keep the required thickness of the active layer for sufficient light absorption.[4]

However, in spite of using a BHJ, the thickness cannot be too large. Above a certain thickness the conversion efficiency drops because free carrier recombination becomes significant.[5] Several approaches have been proposed and reported to overcome weak absorption of OSCs: folded structures,[6] tandem cell architectures,[7] new materials for the active layer,[8,9] and metallic nanoparticles (MNPs).[10–15]

It is known that the localized plasmon resonance in MNPs can cause near-field enhancement and enhanced scattering cross section, and both of them can be used to enhance the absorption in a solar cell. Several experiments and numerical investigations on the influence of MNPs in inorganic solar cells have been performed.[16–22] However, for OSCs most of the investigations on MNPs were based on experiments. In these experiments, absorption and efficiency enhancements have been observed. MNPs were embedded between the anode and the active layer,[10,12,13] between tandem cells,[11] between active layer and cathode,[13] and inside the active layer.[15]

Duche *et al.*[15] investigated the absorption enhancement induced by silver MNPs within the OSC active layer both by experiments and finite-difference time-domain (FDTD)

simulations. However, they only modeled a thin film of active layer with MNPs in three–dimensional (3D). Here we model a more concrete solar cell structure with cathode, active layer and anode based on the finite element method (FEM). We reduce the 3D problem to a two–dimensional (2D) one, since for simulations concerning nanoparticles researchers have shown that a 2D model can give similar results to a 3D model.[23] The advantages of this reduction are of course computational time and memory saving, and it allows us to investigate a larger parameter space in more detail. Furthermore, FEM makes it possible to take the full material dispersion into account as it is a frequency domain method.

In this paper, we present a systematic study on absorption enhancement by embedding a MNP array in the active layer of OSCs based on a 2D model. The simulation setup is discussed in Sec. II. Then in Sec. III we discuss how different parameters of the MNP array such as the spacing between neighboring nanoparticles, the particle diameter, and the coating thickness affect the enhancement. In addition we investigate the enhancement mechanism and analyze the absorption spectra in detail. Finally, we show the optimized parameters of the MNP array with good enhancement.

II. SIMULATION SETUP

In the simulations, due to the indium scarcity, an indium tin oxide (ITO)-free structure[24] was used as shown in Fig. 1. The ITO was replaced by highly conductive polymer, poly (3, 4-ethylenedioxythiophene): poly(styrenesulfonate) (PEDOT:PSS) with 20 nm thickness, which is a polymer with good thermal and chemical stability and good flexibility. For the active layer the commonly used polymer, poly(3-exylthiophene):(6,6)-phenyl-C61-butyric-acid-methyl ester (P3HT:PCBM) with 1:1 weight ratio was used. The material of the cathode is aluminum and the MNPs are silver. The material properties of PEDOT:PSS, silver, aluminum, and P3HT:PCBM are taken from literature.[6,25,26] For the silver

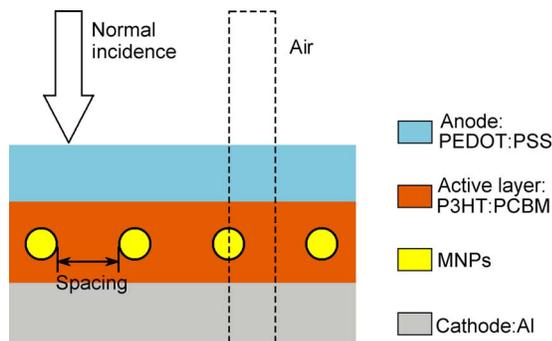a)Electronic addresses: honghui.shen@intec.ugent.be and honghuishen@gmail.com.

FIG. 1. (Color online) Schematic figure of the model of the solar cell with MNPs. In simulations only the dotted domain is used.

FIG. 3. (Color online) Thickness dependence of absorption in the active layer. The inset shows the absorption spectra for active layers with varying thicknesses.

MNPs the influence of the free path effect[11,27] on the dielectric constant is taken into account. Figure 2 shows the refractive indices of the anode and the active material. For the active material the absorption is mainly between 300 and 650 nm.

Here we use a 2D model, so the MNPs are a periodic array of cylindrical nanowires, which are embedded in the middle of the active layer in all simulations. Computations were performed using the commercial fully vectorial COMSOL software package. Light with electric field normal to the nanowires is normally incident from the air into the solar cell (see Fig. 1), passing the PEDOT:PSS, the active layer, and then reaching the cathode. Some light is absorbed in the anode, the active layer, and the cathode, and the rest of it is reflected away from the solar cell.

Due to the periodicity and symmetry of the structure, in order to save computer memory and computational time, only part of the solar cell containing half of the MNPs and half of the space between the MNPs is used, as shown by the
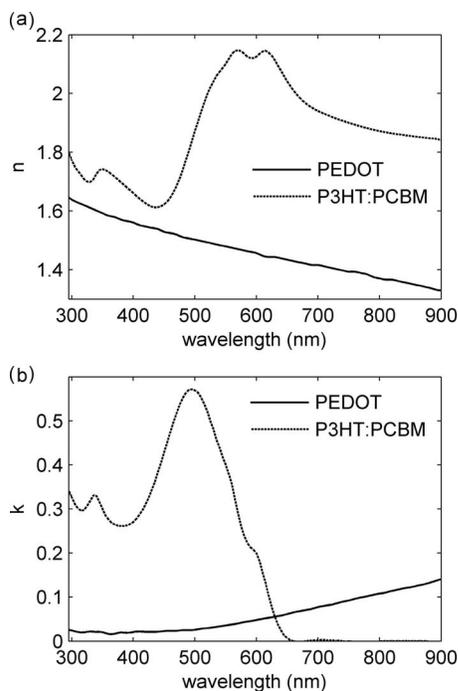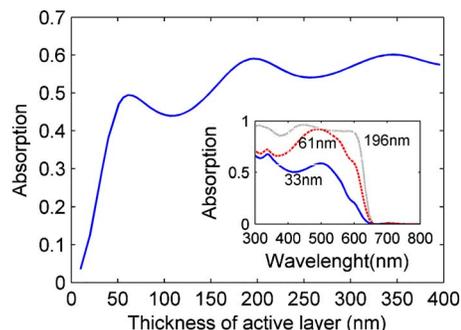
dotted domain in Fig. 1. In simulations a mesh size of around 0.1 nm in the vicinity of the MNPs is employed. Computations have been performed using monochromatic excitations over the wavelength interval 300–800 nm.

III. RESULTS

A. Active layer thickness

We first study solar cells without MNPs and investigate the influence of the active layer thickness on the absorption. The absorption spectrum in the active layer can be obtained directly with COMSOL. The whole absorption over 300–800 nm is then calculated by integrating the absorption spectrum weighted by the AM 1.5G solar spectrum. Figure 3 shows the absorption as a function of the active layer thickness. It can be seen that the absorption oscillates in function of thickness due to interference effects for active layers thicker than 40 nm. For thin active layers interference effects are negligible. Maxima are observed at 61 nm (50%), 196 nm (59%), and 346 nm (60%). From the inset of Fig. 3, it is clear that, over 300–650 nm, solar cells with 196 nm active layer can absorb most of the incident light.

Clearly, thick active layers can absorb most of the incident light. However, as the thickness increases, carrier recombination will become significant, which reduces the internal quantum efficiency. Thin active layers have the advantages of material savings and a high carrier collection efficiency, but at the cost of low light harvesting. However, for solar cells with thin active layers, the light harvesting can be increased by introducing MNPs into the active layer. In this way OSCs could combine the advantages of thin and thick active layers, namely, high carrier collection efficiency and strong light harvesting, resulting in efficient cells.

In what follows, we investigate the influence of MNPs on absorption enhancement for a thin active layer with a thickness of 33 nm. The absorption for this thickness is 30%, and the absorption spectrum is shown in the inset of Fig. 3.

B. Particle spacing

In order to reveal the mechanism of absorption enhancement for a representative case, the diameter of the MNPs is fixed at 10 nm. The diameter influence is discussed in Sec. III D. Figure 4 shows the absorption enhancement (ratio of absorption with MNPs to that without MNPs) in the active

FIG. 2. Real part (a) and imaginary part (b) of refractive indices of PEDOT and P3HT:PCBM (1:1).
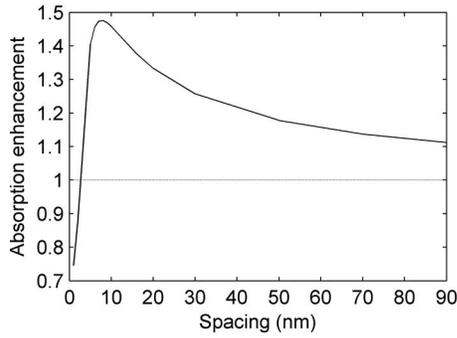
FIG. 4. Absorption enhancement with MNPs in function of particle spacing.

layer (so it does not include the absorption in the MNPs) in function of MNP spacing. The spacing is the distance between neighboring MNPs as defined in Fig. 1. Figure 5 shows the average E field enhancement (E_e) and average mode area (A_m), which is calculated in the active layer (not taking the field inside MNPs into account) over the wavelength interval 300–800 nm using a period of the periodic structure shown in Fig. 1,

$$E_e = \frac{\int \int \int \frac{|E_w|}{|E_{wo}|} dxdyd\lambda}{S\Delta\lambda},$$

$$A_m = \frac{1}{\Delta\lambda} \int \frac{(\int\int |E_w|^2 dxdy)^2}{\int\int |E_w|^4 dxdy} d\lambda,$$

where E_w and E_{wo} are the electric fields with and without MNPs in the active layer, respectively. S denotes the area of active layer except that of MNPs. $\Delta\lambda$ is the wavelength interval and corresponds to 500 nm (from 300 to 800 nm).

Figure 4 shows that there exists an optimum spacing of 8 nm maximizing the absorption enhancement with a factor of around 1.48. This result is clarified by the graphs in Fig. 5. As the spacing increases, the electric field enhancement gets smaller and smaller. However, the field enhancement begins to spread out as the surface plasmon average mode area increases (also shown in Fig. 5). This is due to the decoupling between neighboring MNPs as illustrated by the insets in Fig. 5. When MNPs are far away from each other, the structure converges to the case with no MNPs, meaning that there is no absorption enhancement. As a consequence of these competing effects, there exists an optimum spacing.
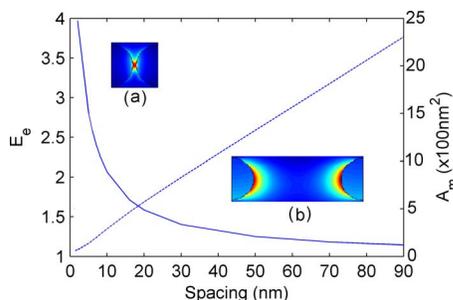

FIG. 5. (Color online) Spacing dependence of average E field enhancement (solid line) and average mode size (dashed line). The insets show the E field enhancement at 425 nm with different spacings: (a) 2 nm and (b) 20 nm.
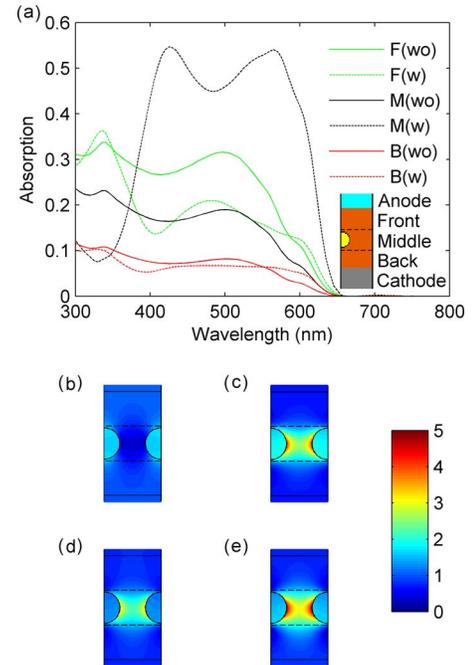

FIG. 6. (Color online) (a) Absorption spectra with (w) and without (wo) MNPs in front (f), middle (m) and back (b) layers with MNPs embedded in the middle layer with 8 nm spacing. Representative figures of electric field enhancement corresponding to 8 nm spacing between MNPs at (b) 330 nm, (c) 425 nm, (d) 485 nm, and (e) 565 nm.

C. Enhancement mechanism

Figure 6(a) shows the absorption spectra. Figures 6(b)–6(e) depict E field enhancement distributions (ratio of the $|E|$ field with MNPs to that without MNPs) at representative wavelengths. In order to reveal which mechanism is more prominent, near field enhancement or enhanced scattering, the active layer is divided into three sublayers: front, middle, and back sublayers, as shown in the inset in Fig. 6(a).

From Fig. 6(a) one observes that the enhanced absorption is obvious only in the middle sublayer where the MNPs are. The black dotted line has a broadband enhancement in the range between around 385 and 650 nm. For the other two sublayers enhanced absorption is only observed in small wavelength ranges while in other ranges the absorption is decreased. These phenomena imply that the absorption enhancement is mainly attributed to near field enhancement and not to enhanced scattering effects.

Figures 6(b)–6(e) show the spatial distributions of the E field enhancement for dips and peaks in the black dotted line in (a), 330, 425, 485, and 565 nm. At 330 nm, due to the small $\text{Re}(\varepsilon_{Ag})$ at short wavelengths, silver loses its metallic properties, and no dipolelike resonance exists at these short wavelengths. For 425, 485, and 565 nm, it is clear that the E field enhancement is mainly localized in the layer where the MNPs are. The maximum enhanced electric field exists in the vicinity of the MNPs in the space between MNPs. Therefore, this also shows that the mechanism of absorption enhancement is mainly due to the enhanced near field, and not to scattering.

From Fig. 6(a) it is also seen that each of the absorption spectra without MNPs (solid lines) has a peak around 485
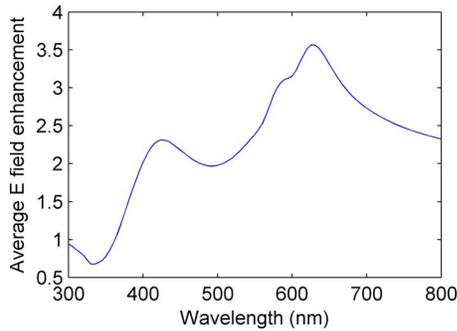
FIG. 7. (Color online) Spectrum of the average E field enhancement for 8 nm spacing between MNPs (when integrated over in the middle sublayer excluding the MNP area).

nm (also shown in the inset to Fig. 3). This is because, as visible in Fig. 1(b), the imaginary part of the P3HT:PCBM index has a peak around 485 nm, which corresponds to a strong absorption at this wavelength. However, when there are MNPs present in the active layer, the absorption at 485 nm decreases, and two peaks appear around 425 and 565 nm. This can be explained as follows.

For a single cylinder nanowire, the resonance position is at 370 nm, which is determined by the quasistatic resonance condition: $Re(\varepsilon_{Ag}) = -Re(\varepsilon_{P3HT:PCBM})$ (when imaginary parts are small).[28] As shown in Fig. 7, which shows an enhancement spectrum, the peak at 425 nm is the redshifted resonance position due to the coupling between neighboring MNPs. This redshifted resonance position determines the absorption peak of the MNP spectra in Fig. 6(a).

It was shown that embedding particles in an absorptive material will suppress the near-field intensity enhancement.[11] The absorption of the active material is large at 485 nm. Therefore, the E field enhancement is lower at 485 nm than at other wavelengths when introducing MNPs into the active layer (see Fig. 7). As a result, the absorption enhancement is also lower there.

From 490 to 630 nm, as shown in Fig. 7, the E field enhancement gets larger. However, for the active material P3HT:PCBM, as shown in Fig. 2(b), the absorption drops in this range. As a consequence, the absorption has another peak around 565 nm.

D. Particle diameter and coating

The dependence of absorption enhancement on the diameter of MNPs has been investigated, as shown by the black solid diamond line in Fig. 8(a). The optimum diameter is 24 nm with an absorption enhancement around 1.56 for 40 nm spacing, as shown in Fig. 8(b). With this diameter and spacing, the solar cell can absorb 47%, which is close to one of the maxima in Fig. 3. There we obtained 50% with a 61 nm active layer without MNPs.

Figure 8(c) shows the absorption spectrum for solar cells with 24 nm diameter MNPs and 40 nm spacing. For comparison, we also plot the absorption spectra for solar cells without MNPs with 33 and 61 nm active layer thickness. We remark that the absorption spectrum of 33 nm active layer with MNPs fits the spectrum of 61 nm active layer without
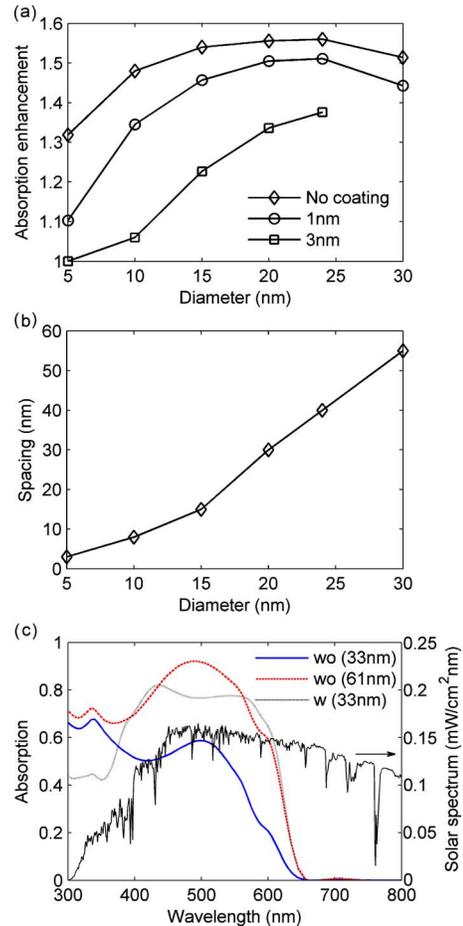

FIG. 8. (Color online) (a) Optimized absorption enhancement as a function of MNP diameter with and without coating. (b) Optimum spacing corresponding to absorption enhancement in (a). (c) Absorption spectra for a solar cell (33 nm) with (w) and without (wo) 24 nm diameter MNPs and for a solar cell (61 nm) without MNPs and AM 1.5G solar spectrum.

MNPs quite well. As a result the absorptions of these cells with (47%) and without (50%) MNPs are similar.

In Fig. 8(a) the influence of coating on absorption enhancement is also depicted. In previous simulations the MNPs were in direct contact with the active layer, therefore the generated excitons can be quenched at the MNPs. In order to avoid this a coating over the MNPs is required. In our numerics silica ($n = 1.46$) is used to coat the MNPs with different thicknesses, see Fig. 8(a). We notice clearly that a thicker coating decreases the absorption enhancement. For MNPs with 5 nm diameter, no enhancement can be observed any more with a 3 nm coating. The coating should be thin compared with the MNP diameter in order to obtain the absorption enhancement.

IV. CONCLUSION

In conclusion, we performed a detailed numerical study on the influence of MNPs for light absorption in OSCs. We analyzed the influence of particle spacing on the absorption. We found that the near field enhancement is the main reason for the absorption enhancement in the active layer. For a thin active layer, such as 33 nm, we noticed that a reasonable particle diameter of about 24 nm is necessary for optimum

absorption enhancement. With this diameter we find the best enhancement with a factor of around 1.56, bringing the structure close to the performance of a much thicker cell without MNPs. In addition, we noticed a strong decline of absorption enhancement as the particle coating thickness increases. Our studies convey a strong interaction between the plasmonic enhancements and the absorption characteristics of the particular active material. Therefore, detailed numerics and experiments for various material configurations are needed to obtain a complete picture of plasmonic enhancement possibilities.

ACKNOWLEDGMENTS

[1]H. Hoppe and N. S. Sariciftci, J. Mater. Res. **19**, 1924 (2004).

[2]J. Peet, J. Y. Kim, N. E. Coates, W. L. Ma, D. Moses, A. J. Heeger, and G. C. Bazan, Nature Mater. **6**, 497 (2007).

[3]S. H. Park, A. Roy, S. Beaupré, S. Cho, N. Coates, J. S. Moon, D. Moses, M. Leclerc, K. Lee, and A. J. Heeger, Nat. Photonics **3**, 297 (2009).

[4]G. Yu, J. Gao, J. C. Hummelen, F. Wudl, and A. J. Heeger, Science **270**, 1789 (1995).

[5]T. Soga, *Nanostructured Materials for Solar Energy Conversion* (Elsevier Science, Amsterdam, 2006).

[6]V. Andersson, K. Tvingstedt, and O. Inganäs, J. Appl. Phys. **103**, 094520 (2008).

[7]J. Y. Kim, K. Lee, N. E. Coates, D. Moses, T. Q. Nguyen, M. Dante, and A. J. Heeger, Science **317**, 222 (2007).

[8]S. R. Forrest, Mater. Res. Bull. **30**, 28 (2005).

[9]W. Y. Wong, X. Z. Wang, Z. He, A. B. Djurisic, C. T. Yip, K. Y. Cheung, H. Wang, C. S. K. Mak, and W. K. Chan, Nature Mater. **6**, 521 (2007).

[10]M. Westphalen, U. Kreibig, J. Rostalski, H. Luth, and D. Meissner, Sol. Energy Mater. Sol. Cells **61**, 97 (2000).

[11]B. P. Rand, P. Peumans, and S. R. Forrest, J. Appl. Phys. **96**, 7519 (2004).

[12]A. J. Morfa, K. L. Rowlen, T. H. Reilly III, M. J. Romero, and J. d. Lagemaatb, Appl. Phys. Lett. **92**, 013504 (2008).

[13]S. S. Kim, S. I. Na, J. Jo, D. Y. Kim, and Y. C. Nah, Appl. Phys. Lett. **93**, 073307 (2008).

[14]X. Chen, C. Zhao, L. Rothberg, and M. K. Ng, Appl. Phys. Lett. **93**, 123302 (2008).

[15]D. Duche, P. Torchio, L. Escoubas, F. Monestier, J. J. Simon, F. Flory, and G. Mathian, Sol. Energy Mater. Sol. Cells **93**, 1377 (2009).

[16]D. Derkacs, S. H. Lim, P. Matheu, W. Mar, and E. T. Yu, Appl. Phys. Lett. **89**, 093103 (2006).

[17]S. Pillai, K. R. Catchpole, T. Trupke, and M. A. Green, J. Appl. Phys. **101**, 093105 (2007).

[18]S. H. Lim, W. Mar, P. Matheu, D. Derkacs, and E. T. Yu, J. Appl. Phys. **101**, 104309 (2007).

[19]K. R. Catchpole and A. Polman, Appl. Phys. Lett. **93**, 191113 (2008).

[20]C. Rockstuhl, S. Fahr, and F. Lederer, J. Appl. Phys. **104**, 123102 (2008).

[21]Y. A. Akimov, W. S. Koh, and K. Ostrikov, Opt. Express **17**, 10195 (2009).

[22]C. Rockstuhl and F. Lederer, Appl. Phys. Lett. **94**, 213102 (2009).

[23]F. Moreno, B. G.-Cámara, J. M. Saiz, and F. González, Opt. Express **16**, 12487 (2008).

[24]B. Zimmermann, M. Glatthaar, M. Niggemann, M. K. Riede, A. Hinsch, and A. Gombert, Sol. Energy Mater. Sol. Cells **91**, 374 (2007).

[25]E. D. Palik, *Handbook of Optical Constants of Solids* (Academic, New York, 1985).

[26]F. Monestier, J. J. Simon, P. Torchio, L. Escoubas, F. Flory, S. Bailly, R. D. Bettignies, S. Guillerez, and C. Defranoux, Sol. Energy Mater. Sol. Cells **91**, 405 (2007).

[27]U. Kreibig and M. Vollmer, *Optical Properties of Metal Clusters* (Springer, Berlin, 1995).

[28]L. Novotny and B. Hecht, *Principles of Nano-Optics* (Cambridge University Press, Cambridge, 2006).